

Coupling a single electron to a Bose-Einstein condensate

Jonathan B. Balewski¹, Alexander T. Krupp¹, Anita Gaj¹, David Peter², Hans Peter Büchler², Robert Löw¹, Sebastian Hofferberth¹ & Tilman Pfau¹

¹*Physikalisches Institut, Universität Stuttgart, Pfaffenwaldring 57, 70569 Stuttgart, Germany*

²*Institut für Theoretische Physik III, Universität Stuttgart, Pfaffenwaldring 57, 70569 Stuttgart, Germany*

The coupling of electrons to matter is at the heart of our understanding of material properties such as electrical conductivity. One of the most intriguing effects is that electron-phonon coupling can lead to the formation of a Cooper pair out of two repelling electrons, the basis for BCS superconductivity¹. Here we study the interaction of a single localized electron with a Bose-Einstein condensate (BEC) and show that it can excite phonons and eventually set the whole condensate into a collective oscillation. We find that the coupling is surprisingly strong as compared to ionic impurities due to the more favorable mass ratio. The electron is held in place by a single charged ionic core forming a Rydberg bound state. This Rydberg electron is described by a wavefunction extending to a size comparable to the dimensions of the BEC, namely up to 8 micrometers. In such a state, corresponding to a principal quantum number of $n=202$, the Rydberg electron is interacting with several tens of thousands of condensed atoms contained within its orbit. We observe surprisingly long lifetimes and finite size effects due to the electron exploring the wings of the BEC. Based on our results we anticipate future experiments on electron wavefunction imaging, investigation of phonon mediated coupling of single electrons, and applications in quantum optics.

Charged impurities were very successfully used as probes for elementary excitations in the early studies of superfluidity in liquid Helium. These applications span the interaction of ion impurities with phonons and rotons², the creation and study of vortex lattices by impurities³, as well as the coupling of electrons to surface ripplons⁴. Additionally they have been proposed for applications in quantum information⁵. The emergence of Bose-Einstein condensation of alkali atoms has renewed the interest in impurity physics. Positively charged impurities in a BEC were first created by Penning ionization of metastable atoms⁶ and photoionization⁷. Recently single ion trapping⁸ allowed for the first time the study of the interaction between a single charged impurity and a BEC in a well controlled manner. Besides bare losses by classical scattering, chemical reactions both with the impurity⁹ as well as

catalytic reactions¹⁰ mediated by the impurity have been observed. Alternatively, the creation of neutral spin impurities in Fermi liquids offers tunable interaction strength with the bulk by means of a Feshbach resonance. A Feshbach resonance allows to change the character of the interaction from free impurities via a quasiparticle state, so called Fermi polarons, to bound diatomic molecules^{11,12}.

For all such impurities, the interaction is inversely proportional to the reduced mass of the impurity and the bulk species¹³. Light impurities such as electrons are therefore, in general, more favorable to obtain strong coupling. However, electrons require an appropriate trapping potential because even the tiniest electric field will lead to a considerable acceleration. The simplest trap for an electron offered by nature is a positively charged nucleus. We use highly excited Rydberg states, where the electron is delocalized over regions of up to several micrometers from the atomic core. At these distances the binding to the core is weak and the Rydberg electron becomes quasi free, making it susceptible to interaction with its environment. Nonetheless, the binding to the ionic core is strong enough to provide sufficient trapping of the electron even in a strongly interacting environment. In fact, Amaldi and Segrè observed Rydberg absorption series in the range of principle quantum numbers around 30 at pressures reaching one atmosphere¹⁴. In this regime the spatial extend of the electron wavefunction is much larger than the mean interparticle distance, causing large interaction induced line shifts and broadenings. The explanation of these effects led to the nowadays well known Fermi pseudopotential¹⁵, describing the short range interaction of the quasi free Rydberg electron at position \mathbf{r} with neutral ground state atoms at \mathbf{R} :

$$V_{\text{pseudo}}(\mathbf{r}, \mathbf{R}) = \frac{2\pi\hbar^2 a}{m_e} \delta(\mathbf{r} - \mathbf{R}) \quad (1)$$

Here the interaction strength is fully characterized by the scattering length a . Given the Rydberg electron wavefunction $\Psi(\mathbf{r})$, the pseudopotential leads to a mean field potential:

$$V(\mathbf{R}) = \frac{2\pi\hbar^2 a}{m_e} |\Psi(\mathbf{R})|^2 \quad (2)$$

The interaction is restricted to a range given by the size of the Rydberg atom $\propto n^2 a_0$, where a_0 denotes the Bohr radius. If this is comparable to the mean interparticle distance this interaction can lead to a bound state¹⁶ in the case of negative scattering lengths a . Diatomic¹⁷ and triatomic molecules¹⁸ of

this class have been experimentally observed for ^{87}Rb atoms at principal quantum numbers in the range of $n = 40$ and densities of the order of 10^{12} cm^{-3} . At higher densities however, the lifetime of these bound states was found to decrease significantly¹⁹.

The experiments described here are performed in a completely different regime. We combine much higher Rydberg states at principal quantum numbers $n = 110 - 202$ with high densities of up to 10^{14} cm^{-3} in a BEC. In this regime, a significant fraction of the BEC is inside the electron orbit. Consequently, the single electron impurity has an impact on the BEC wavefunction as a whole. We vary the absolute number of atoms inside the electron orbit from 700 to up to 30,000 by changing the principal quantum number which increases the spatial extent of the electron wavefunction up to the wings of the condensate (see Fig. 1).

We start with a magnetically trapped Bose-Einstein condensate of ^{87}Rb atoms in the $|5S_{1/2}, m_F = 2\rangle$ state. We illuminate the BEC with light from two lasers coupling the ground state to the $|nS_{1/2}, m_S = 1/2\rangle$ state ($n = 110 - 202$) via the intermediate $5P_{3/2}$ state (see Methods). The strong van-der-Waals interaction between Rydberg atoms in such high states prevents the simultaneous excitation of two Rydberg atoms within a certain distance r_B . For Rydberg states with $n > 100$ this blockade effect²⁰ allows only a single Rydberg excitation in the whole BEC, since the blockade radius here is significantly larger than the Thomas-Fermi radii of the condensate (see Fig. 1a and Supplementary Information). This enables us to create one single electron impurity in the condensate. After a defined interaction time on the order of the Rydberg state lifetime, we apply an electric field pulse to remove the ionic core as well as the electron. We repeat this sequence several hundred times in a single condensate, before releasing the BEC and taking an absorption image after 50 ms time of flight. The long expansion time isolates the low momentum components of the trapped atom cloud, as the free particles have already traveled out of the region of interest. From these time of flight images we extract the change in atom number and the aspect ratio of the BEC at different detunings of the excitation lasers relative to the single atom Rydberg level and different principal quantum numbers (see Fig. 2).

We observe the impact of the electron impurity as a loss of atoms from the BEC after time of flight. Compared to the Rydberg resonances measured in a thermal cloud at low densities the observed lines in the BEC are shifted to the red inversely proportional to the Rydberg quantum number. We can explain this shift by the low energy scattering of the electron from the BEC atoms. While the mean depth of the interaction potential decreases from 12 kHz to 290 Hz with increasing principal quantum number, the number of atoms inside the electron wavefunction increases. Integrating the mean field

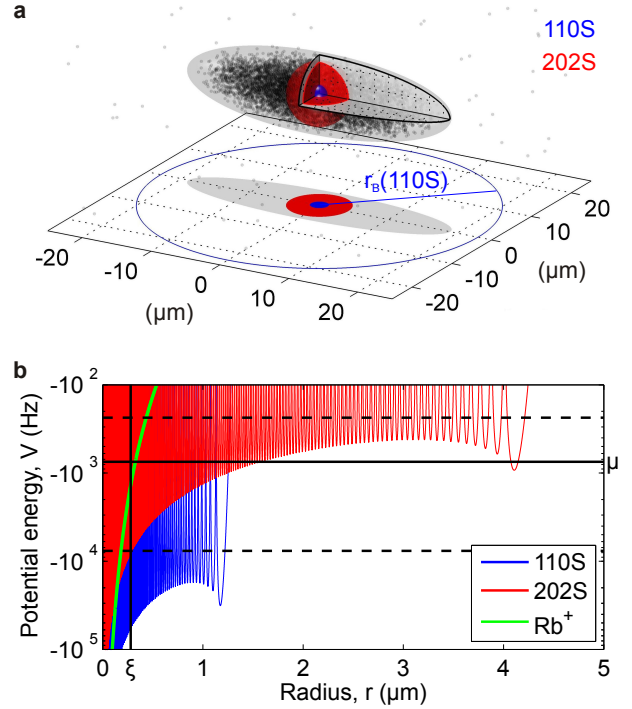


Figure 1: Size comparison in the spatial and energy domains. **a** Depending on the Rydberg state the electron impurity is localized in different volumes in a Bose-Einstein condensate consisting of $N = 8 \cdot 10^4$ atoms. The sizes of the lowest (110S, blue) and highest Rydberg state (202S, red) under investigation are indicated. The densities of the BEC and the surrounding thermal cloud are to scale. The lower bound of the blockade radius r_B for the 110S state is denoted as a blue circle in the projection. The blockade radii for the higher Rydberg states are off the scale. **b** The corresponding interaction potentials $V(r)$ from equation (2) are orders of magnitude stronger than the contribution of the positively charged Rydberg core (green) except for very small distances. The mean interaction strength (black dashed lines) can be set below and above the chemical potential $\mu = 745 \text{ Hz}$ of the condensate (horizontal black line) by choosing the Rydberg state. The healing length $\xi = 274 \text{ nm}$ of the condensate (vertical black line) is much smaller than the spatial extent of the electron wavefunction.

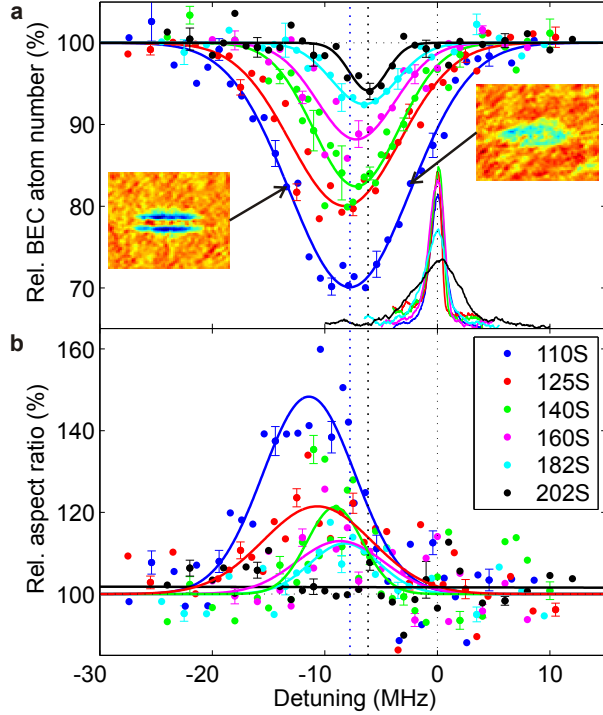


Figure 2: Rydberg excitation spectra for different principal quantum numbers. Relative change of the BEC atom number (a) and aspect ratio (b) after time of flight. The solid lines are Gaussian fits to the data. The zero position is determined as the position of the Rydberg line in the thermal cloud, as shown for reference. The change of aspect ratio is illustrated in the insets of a, which show difference pictures of the condensate at two distinct spectral positions of the 110S state, where the overall losses (blue) are the same. Due to the deformation the condensate gets more elongated, compensating for the atom losses in the center. For the measurements at the two lowest Rydberg states, $n = 110$ and 125 a Rydberg atom was excited 300 times; for the other states 500 repetitions were chosen. The exemplary error bars are the standard deviation from ten independent measurements.

potential $V(\mathbf{R})$ over all atoms inside the Rydberg electron wavefunction we obtain the total shift, which depends to lowest order^{14,15} only on the mean atomic density \bar{n} :

$$\Delta E = \int_{\text{Ryd}} d^3R V(\mathbf{R})n(\mathbf{R}) = \frac{2\pi\hbar^2 a}{m_e} \bar{n} \quad (3)$$

For homogeneous densities the shift is therefore independent of the actual Rydberg state. This is consistent with our measurements at smaller principal quantum numbers where the

local density approximation is fulfilled. For higher principal quantum numbers however, we find a significant deviation. When the spatial extent of the Rydberg atom becomes comparable to the radial size of the BEC (see Fig. 1a), the electron is exploring mainly the low density wings of the condensate. We can account for this by averaging the Thomas-Fermi density distribution over the size of the Rydberg atom. We assume the Rydberg atom is being excited in the center of the condensate and use the average value of the peak density $\bar{n} = 8.6 \cdot 10^{13} \text{ cm}^{-3}$ over one sequence. In Fig. 3a the calculated shift is plotted in comparison to the line shifts extracted from Fig. 2a. In addition to the values for a constant scattering length²¹ of $a = -16.1 a_0$, a calculation taking higher order scattering theory into account is shown in Fig. 3c (see Supplementary Information). This simple model without any fit parameters quantitatively agrees remarkably well with our data.

The density dependent shift of the Rydberg line allows us to control the position of the electron impurity inside the BEC much better than our optical resolution simply by changing the frequency of the excitation lasers. This is confirmed by the measured deformation of the condensate (Fig. 2b). The interaction of the electron impurity with the BEC excites a quadrupole shape oscillation that leads to a change in the aspect ratio after time of flight. In particular, we observe the strongest deformation on the red side of the BEC loss feature, i.e. in the region of largest density-induced shift. Here the electron impurity is localized at the center of the condensate and strong deformation of the condensate can be expected, whereas on the blue side and at high principal quantum numbers the mechanical effect averages to zero for repeated excitations. A quantitative modeling of this effect however, is more involved and is subject to future studies.

In order to determine the actual interaction time of an individual impurity with the BEC we measure the lifetime of the Rydberg atoms (see Fig. 3b and Supplementary Information). From empirical scaling laws²² one would expect the Rydberg lifetimes τ to increase with principal quantum number as n^3 , here from 1.7 ms ($n = 110$) to 10.8 ms ($n = 202$). However, we already observe a reduced lifetime of around 780 μs at densities around 10^{12} cm^{-3} in the thermal cloud for all Rydberg states investigated between $n = 110$ and 202. In the condensate, at peak densities just below 10^{14} cm^{-3} , we find the lifetime to be further reduced by about two orders of magnitude. In this high density regime we observe a lifetime increasing with principal quantum number. These two observations suggest that there is a dominant decay mechanism which is mainly dependent upon the density of the background gas. Further discussion of this effect can be found in the Supplementary Information.

We now turn to the quantitative analysis of the fraction of

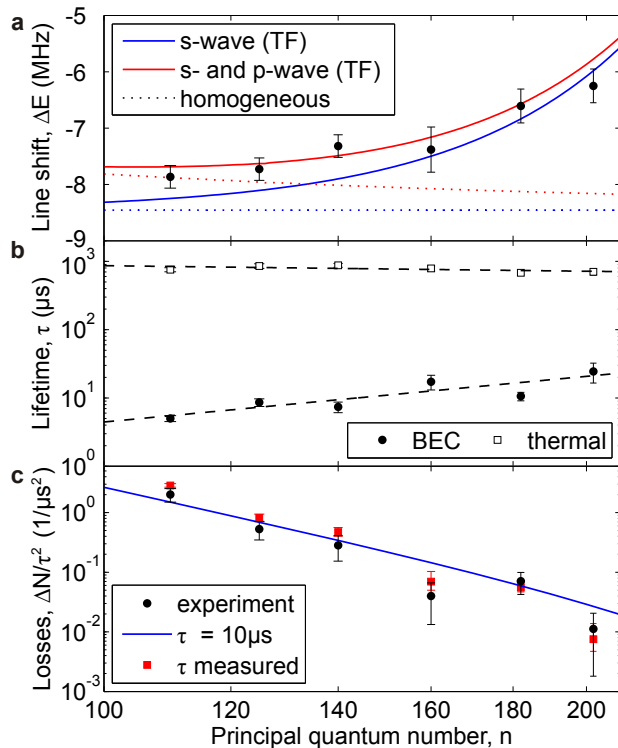


Figure 3: Energy shift and lifetime reduction of the Rydberg state in a condensate and Rydberg electron induced loss of BEC atoms. **a** Theory curves with constant s-wave scattering length (blue) and taking higher order corrections into account (red) are shown. The corresponding values neglecting the Thomas-Fermi density distribution are indicated as dotted lines. The dashed lines in **b** are power law fits to measurements in the condensate (circles) and the thermal cloud (squares). In **c** the atom loss from Fig. 2a is divided by the square of the Rydberg lifetime τ in the condensate. Theory values taking the measured lifetime into account (red squares) and assuming a constant lifetime of $10\mu\text{s}$ (blue line) are shown. Error bars are 68% confidence bounds of Gaussian fits from Fig. 2a (**a**), exponential fits to the measured decay (**b**) and the combination of both (**c**).

atoms removed from the condensate due to the electron impurity. To fully model this process we have to take the coherent properties of the condensate and its excitations into account. We use perturbation theory to calculate the number of excitations in the condensate. Expressing the interaction potential $V(\mathbf{r})$ from equation (2) in terms of Fourier components $\rho_{\mathbf{q}} = \int d^3r e^{-i\mathbf{q}\mathbf{r}} |\Psi(\mathbf{r})|^2$ of the electron density, the relevant

part of the interaction reads (see Supplementary Information):

$$\hat{H}_{\text{int}} = \frac{2\pi\hbar^2 a}{m_e} \frac{\bar{n}}{\sqrt{N}} \sum_{\mathbf{q} \neq 0} \rho_{\mathbf{q}} (u_{\mathbf{q}} - v_{\mathbf{q}}) (\hat{b}_{\mathbf{q}}^\dagger + \hat{b}_{-\mathbf{q}}) \quad (4)$$

where $u_{\mathbf{q}}$ and $v_{\mathbf{q}}$ denote the Bogoliubov factors and $\hat{b}_{\mathbf{q}}^\dagger$ is the creation operator of a collective excitation with quasi momentum \mathbf{q} . The characteristic length scale of the interaction potential is given by the outer edge located at about the Bohr orbit $\propto n^2 a_0$. This length scale is larger than the healing length of the BEC for all Rydberg states investigated here (see Fig. 1b). Therefore, a significant part of the excitations are created in the phonon regime. After time of flight both phonon and free particle excitations can be detected as atom losses. Furthermore, the interaction time of each Rydberg electron with the condensate is finite, limited by its lifetime and the experimental sequence. Taking these corrections into account (see Supplementary Information), we are able to reproduce our experimental results. Fig. 3c shows the maximum atom loss extracted from the data in Fig. 2a, divided by the square of the lifetimes τ measured for each Rydberg state. This way we remove the main dependency on τ (see Supplementary Information). The solid line shows the atom loss predicted by our Bogoliubov calculation assuming a constant lifetime of $\tau = 10\mu\text{s}$ for all Rydberg states. This already reproduces the overall effect very well. Even better agreement between our data and theory can be achieved if we use the explicitly measured lifetime of each Rydberg state (red points in Fig. 3c).

In view of our results on the coupling of a single electron to BEC excitations further phenomena like trapping of a whole condensate by an impurity come within reach. A repulsive interaction between electron and BEC could be achieved by changing the spin state of the electron. Tiny electric fields are sufficient to deform and manipulate the Rydberg electron wavefunction offering further options to control the coupling. The interaction of the impurity with excitations already present in the condensate could provide a model system for phonon mediated coupling of electrons. From the perspective of the single Rydberg atom the strong interaction of the excited electron with the background gas opens the possibility of manipulating its quantum mechanical state as well as its motional degrees of freedom. These effects enable intriguing quantum optics applications. For example, the scattering from the background gas could serve as a source of dephasing, forming a crucial part in the proposal for a single photon absorber²³. Finally, the BEC provides a sensitive probe for individual Rydberg atoms since the depletion of the BEC is localized inside the volume of the electron wavefunction. Highly ordered quasi crystalline samples of multiple Rydberg atoms in one condensate or even two overlapping Rydberg atoms could be created and probed by means of double res-

onance spectroscopy²⁴. Making use of well established techniques like in-situ phase contrast imaging, even the imaging of a single electron orbital seems feasible.

Methods

We start with a condensate of $N = 8 \cdot 10^4$ ^{87}Rb atoms in the $|5S_{1/2}, m_F = 2\rangle$ state in a cloverleaf type magnetic trap at a high magnetic offset field of 1.355 mT (radial/axial trap frequencies $\omega_\rho = 2\pi \cdot 81.7$ Hz and $\omega_z = 2\pi \cdot 22.4$ Hz). We excite Rydberg states $|nS_{1/2}, m_S = 1/2\rangle$ ($n = 110 - 202$) via a two-photon transition detuned by 500 MHz from the intermediate $5P_{3/2}$ state using continuous wave diode lasers at 780 nm and 480 nm. The blue laser beam has a power of 100 mW and is focused down to a size of $60 \mu\text{m}$ ($1/e^2$ diameter). We choose the power of the red beam typically in the range of $3 \mu\text{W}$ at a diameter of $500 \mu\text{m}$ ($1/e^2$). The two laser beams are shone in counterpropagating along the magnetic field axis of the trap. We address the desired transition by choosing σ^+ and σ^- polarization for the 780 nm and 480 nm laser respectively.

In each condensate a sequence consisting of a $1 \mu\text{s}$ light pulse for Rydberg excitation and a $2 \mu\text{s}$ electric field pulse for removal of any remaining Rydberg atoms or ions, separated by $10 \mu\text{s}$ delay time, is repeated 300-500 times at a rate of 62.5 kHz. The clearance field is set to 5.7 V/cm, well above the ionization threshold of all Rydberg states under investigation. After a time of flight of 50 ms we take an absorption image of the condensate. We determine the relative change in atom number and aspect ratio by comparing each measurement with a consecutive reference image where the blue Rydberg laser is detuned by more than 40 MHz.

Further details about the setup and the data analysis can be found in ref. 25 and in the Supplementary Information.

1. Bardeen, J., Cooper, L. N. & Schrieffer, J. R. Theory of superconductivity. *Phys. Rev.* **108**, 1175–1204 (1957).
2. Reif, F. & Meyer, L. Study of superfluidity in liquid He by ion motion. *Phys. Rev.* **119**, 1164–1173 (1960).
3. Rayfield, G. W. & Reif, F. Evidence for the creation and motion of quantized vortex rings in superfluid helium. *Phys. Rev. Lett.* **11**, 305–308 (1963).
4. Fisher, D. S., Halperin, B. I. & Platzman, P. M. Phonon-rippion coupling and the two-dimensional electron solid on a liquid-helium surface. *Phys. Rev. Lett.* **42**, 798–801 (1979).
5. Platzman, P. M. & Dykman, M. I. Quantum computing with electrons floating on liquid helium. *Science* **284**, 1967–1969 (1999).
6. Robert, A. *et al.* A Bose-Einstein condensate of metastable atoms. *Science* **292**, 461–464 (2001).
7. Ciampini, D. *et al.* Photoionization of ultracold and Bose-Einstein-condensed Rb atoms. *Phys. Rev. A* **66**, 043409 (2002).
8. Zipkes, C., Palzer, S., Sias, C. & Köhl, M. A trapped single ion inside a Bose-Einstein condensate. *Nature* **464**, 388–391 (2010).
9. Ratschbacher, L., Zipkes, C., Sias, C. & Köhl, M. Controlling chemical reactions of a single particle. *Nature Physics* **8**, 649–652 (2012).
10. Härter, A. *et al.* Single ion as a three-body reaction center in an ultracold atomic gas. *Phys. Rev. Lett.* **109**, 123201 (2012).
11. Shin, Y., Schunck, C. H., Schirotzek, A. & Ketterle, W. Tomographic rf spectroscopy of a trapped fermi gas at unitarity. *Phys. Rev. Lett.* **99**, 090403 (2007).
12. Schirotzek, A., Wu, C.-H., Sommer, A. & Zwierlein, M. W. Observation of fermi polarons in a tunable fermi liquid of ultracold atoms. *Phys. Rev. Lett.* **102**, 230402 (2009).
13. Massignan, P., Pethick, C. J. & Smith, H. Static properties of positive ions in atomic Bose-Einstein condensates. *Phys. Rev. A* **71**, 023606 (2005).
14. Amaldi, E. & Segrè, E. Effect of pressure on high terms of alkaline spectra. *Nature* **133**, 141 (1934).
15. Fermi, E. Sopra lo spostamento per pressione delle righe elevate delle serie spettrali. *Nuovo Cimento* **11**, 157–166 (1934).
16. Greene, C. H., Dickinson, A. S. & Sadeghpour, H. R. Creation of polar and nonpolar ultra-long-range Rydberg molecules. *Phys. Rev. Lett.* **85**, 2458–2461 (2000).
17. Bendkowsky, V. *et al.* Observation of ultralong-range Rydberg molecules. *Nature* **458**, 1005–1008 (2009).
18. Bendkowsky, V. *et al.* Rydberg trimers and excited dimers bound by internal quantum reflection. *Phys. Rev. Lett.* **105**, 163201 (2010).

19. Butscher, B. *et al.* Lifetimes of ultralong-range Rydberg molecules in vibrational ground and excited states. *Journal of Physics B: Atomic, Molecular and Optical Physics* **44**, 184004 (2011).
20. Saffman, M., Walker, T. G. & Mølmer, K. Quantum information with Rydberg atoms. *Reviews of Modern Physics* **82**, 2313–2363 (2010).
21. Bahrim, C., Thumm, U. & Fabrikant, I. I. 3S_e and 1S_e scattering lengths for $e^- + \text{Rb}$, Cs and Fr collisions. *Journal of Physics B: Atomic, Molecular and Optical Physics* **34**, L195 (2001).
22. Beterov, I. I., Ryabtsev, I. I., Tretyakov, D. B. & Entin, V. M. Quasiclassical calculations of blackbody-radiation-induced depopulation rates and effective lifetimes of Rydberg ns , np , and nd alkali-metal atoms with $n \leq 80$. *Phys. Rev. A* **79**, 052504 (2009).
23. Honer, J., Löw, R., Weimer, H., Pfau, T. & Büchler, H. P. Artificial atoms can do more than atoms: Deterministic single photon subtraction from arbitrary light fields. *Phys. Rev. Lett.* **107**, 093601 (2011).
24. Reinhard, A. *et al.* Double-resonance spectroscopy of interacting Rydberg-atom systems. *Phys. Rev. Lett.* **100**, 233201 (2008).
25. Löw, R. *et al.* An experimental and theoretical guide to strongly interacting Rydberg gases. *Journal of Physics B: Atomic, Molecular and Optical Physics* **45**, 113001 (2012).
26. Heidemann, R. *et al.* Evidence for coherent collective Rydberg excitation in the strong blockade regime. *Phys. Rev. Lett.* **99**, 163601 (2007).
27. Hickman, A. P. Relation between low-energy-electron scattering and l -changing collisions of Rydberg atoms. *Phys. Rev. A* **19**, 994–1003 (1979).
28. Barbier, L., Djerad, M. T. & Chéret, M. Collisional ion-pair formation in an excited alkali-metal vapor. *Phys. Rev. A* **34**, 2710–2718 (1986).
29. Omont, A. On the theory of collisions of atoms in Rydberg states with neutral particles. *J. Phys. France* **38**, 1343–1359 (1977).

Deutsche Forschungsgemeinschaft (DFG) within the SFB/TRR21 and the project PF 381/4-2. We also acknowledge support by the ERC under contract number 267100 and A.G. acknowledges support from E.U. Marie Curie program ITN-Coherence 265031.

Acknowledgements We would like to thank K. Rzażewski and J. Hecker Denschlag for valuable discussions and C. Tresp for setting up the Rydberg laser system. This work is funded by the

Supplementary Information

1 Thermal cloud data

The reference measurements of the unperturbed Rydberg state in the thermal cloud were performed with a sample of $2 \cdot 10^6$ atoms at a temperature of $2.6 \mu\text{K}$. The spectra were taken by laser excitation and subsequent field ionization and ion detection²⁵. The electric field for ionization was 5.7 V/cm throughout all measurements, which is well above the classical ionization threshold of 2.5 V/cm . A complete spectrum was taken in one atomic sample by repeating the cycle of excitation and detection 401 times at a rate of 167 Hz while varying the laser detuning on each shot. The lines shown in Fig. 2a were obtained by averaging 20 spectra. For these spectra a long excitation pulse length of $100 \mu\text{s}$ and low red powers of few nW were chosen to minimize linewidth. This linewidth, increasing from just below 1 MHz at $n = 110$ to about 5 MHz at $n = 202$, is clearly limited by the electric field control. We compensated stray electric fields by repeatedly taking Stark parabola along three axes. We estimate the level of electric field control to be on the order of 1 mV/cm . The measured linewidth increased at slightly higher temperatures of the atomic sample, indicating the presence of residual electric field gradients. We expect much smaller line broadening caused by inhomogeneous fields in the BEC due to its smaller spatial extent.

For the lifetime measurements in Fig. 3b spectra with varying time delay between excitation and detection were taken. Here the same power as for the corresponding condensate measurements was used with pulse lengths of 1 to $4 \mu\text{s}$ to obtain a constant signal amplitude for all Rydberg states. For each delay time 5 spectra were averaged and the amplitude extracted by a Gaussian fit.

2 BEC data

To study the effect of a single Rydberg electron on the condensate a sequence consisting of a $1 \mu\text{s}$ long Rydberg excitation pulse and a $2 \mu\text{s}$ long field ionization pulse, with a fixed delay time of $10 \mu\text{s}$ in between, was repeated 300-500 times at a rate of 62.5 kHz . The red power was adjusted for each principal quantum number in the range of around $3 \mu\text{W}$ to the plateau value of a saturation curve²⁶. After a time of flight of 50 ms an absorption image was taken from which the atom number and aspect ratio of the BEC was extracted. We determine the atom number by summing all pixels in a rectangle around the condensate and normalizing the number for each picture onto the average background signal in a region without atoms. The aspect ratio was obtained from a one dimensional Thomas-Fermi fit to slices integrated along 11 pixels (pixel size $6.45 \mu\text{m}$) along the long and short axis of the condensate.

During each sequence, the number of atoms in the condensate decreased from $8 \cdot 10^4$ to around $5 \cdot 10^4$ atoms, even in the absence of Rydberg excitations, mainly due to off-resonant scattering from the intermediate $5P_{3/2}$ state and heating. To eliminate this effect from the data, as well as to reduce the effect of drifts in atom number and deformation during time of flight originating from residual magnetic field gradients, the data from each absorption image was related to a reference measurement taken immediately before or after where the blue Rydberg laser was detuned by more than 40 MHz . Therefore any Rydberg excitation was avoided while keeping the loss due to the red Rydberg laser and the deformation due to the focused blue Rydberg laser constant. For each data point in Fig. 2 ten measurements were averaged. For the insets in Fig. 2 we subtracted the reference image from the image with Rydberg excitation and averaged again over ten repetitions. Note that taking one BEC spectrum as in Fig. 2 takes therefore at least ten hours of uninterrupted measurement time without preparation and warming up, while an averaged spectrum in the thermal cloud can be obtained easily within ten minutes at much better resolution. We monitored the initial BEC atom number during the experiments and it turns out that small drifts are negligible except for the measured line shift of the Rydberg state. Therefore we normalize the line positions extracted from Fig. 2a to the mean peak density $\propto N^{2/5}$ to obtain the values shown in Fig. 3a.

For the lifetime measurements in Fig. 3b the delay time between excitation and ionization was varied. The detuning of the Rydberg lasers was set to the position of maximum atom loss in Fig. 2. The overall length of the sequence was adapted to the maximum delay time but kept constant throughout the measurement of one Rydberg state. For the longest delay times we

found no change of the measured BEC atom losses if we switched the field ionization off. From this we can conclude that we really detect the decay of the Rydberg atom itself and not only the decay of its effect on the condensate.

3 Effect of impurity atom mass ratio on interaction strength

In the main paper we state that light impurities in general cause a stronger interaction with the bulk. A thermodynamic consideration based on ref. 13 provides an estimate of the excess number of atoms ΔN which is accumulated around a single impurity in equilibrium. This number can be expressed in terms of the reduced masses m and scattering lengths a for the atom-atom (aa) and atom-impurity (ai) scattering respectively:

$$\Delta N = -\frac{m_{aa} a_{ai}}{m_{ai} a_{aa}} \quad (5)$$

The atom-impurity scattering length a_{ai} itself is also a function of the reduced mass m_{ai} . The order of magnitude for a singly charged impurity interacting with atoms with polarizability α can be estimated as the characteristic radius r_{ai} of the polarization potential⁸:

$$r_{ai} = \sqrt{\frac{m_{ai}\alpha e^2}{(4\pi\epsilon_0\hbar)^2}} \quad (6)$$

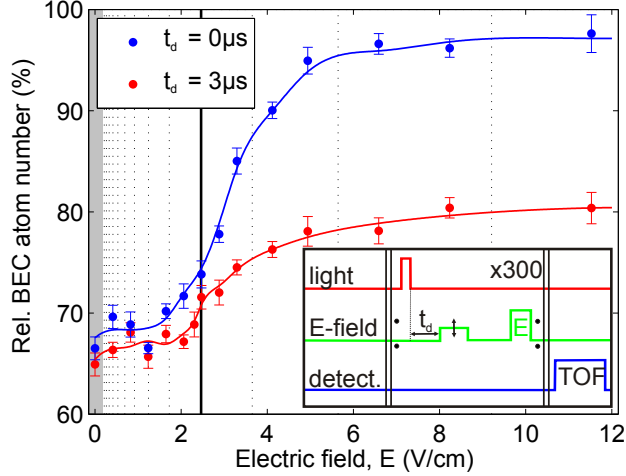
The absolute value of $r_{ai} = 18.0 a_0$ agrees quite well with the actual value of $a_{ai} = -16.1 a_0$ for the e^- -⁸⁷Rb triplet scattering observed in this paper, whereas the singlet scattering length $a_{ai} = 0.627 a_0$ differs considerably²¹. This leads to a scaling of $\Delta N \propto 1/\sqrt{m_{ai}}$. In case of ⁸⁷Rb one can therefore expect the effect of an electron impurity to be about a factor of 400 stronger than that of a positively charged ion of the same element as the bulk atoms. The value of ΔN then exceeds one thousand. Here we are clearly reaching the limits of weak perturbation assumed in the derivation of ΔN .

4 Blockade radius

The interaction between two Rydberg atoms in an S state is a purely repulsive van-der-Waals interaction C_6/r^6 except for very small interatomic distances r . In the main paper we state the minimum distance between two Rydberg atoms which can still be excited with one laser at fixed center frequency f but with finite linewidth Δf , the blockade radius r_B . As a simple estimate for the blockade radius we equate the van-der-Waals interaction with the linewidth Δf and obtain:

$$r_B \approx \sqrt[6]{C_6/(h\Delta f)} \quad (7)$$

As discussed above, this linewidth is dominated by electric field gradients which are expected to play a much smaller role on BEC length scales. Therefore, the actual blockade radius around one Rydberg atom in the condensate is expected to be much larger than estimated. However, we note that this simple picture of the Rydberg blockade in our case has to be extended by the density dependent line shift according to equation (3) which can cause an antiblockade effect. Since the van-der-Waals interaction is purely repulsive a Rydberg excitation in the low density region of the condensate, at a detuning close to zero with respect to the thermal cloud, could possibly tune a second excitation more in the center of the BEC into resonance. The zero crossings of the combined interaction and density dependent potentials, therefore, in principle allow to create quasi crystalline ordered structures of Rydberg atoms. More important for the work presented here, however, is that for large detunings Rydberg atoms are excited preferentially in the center of the condensate. In this case the density gradient and the Rydberg-Rydberg interaction are of the same sign and there is consequently no antiblockade effect present. On the contrary, the blockade by a single excitation here is even more effective.



Supplementary Figure 1: Study of Rydberg decay of the 110S state. The BEC atom loss was measured varying the electric field strength of pulses with a delay time of $t_d = 3 \mu\text{s}$ (red) and immediately after Rydberg excitation (blue). The dotted vertical lines indicate the classical ionization threshold for Rydberg states in steps of ten principal quantum numbers. The solid black line corresponds to the value for $n = 110$. In the grey shaded area the electric field is not strong enough to extract a possibly existing ion from the condensate during the electric field pulse. The experimental sequence is depicted in the inset.

5 Rydberg decay

We observe shorter lifetimes of Rydberg states than expected from spontaneous decay only (see Fig. 3b). Furthermore, the comparison between measurements in the thermal cloud and in the condensate suggest a linear dependence on the density of ground state atoms. Initially one could therefore expect that the weak binding of the highly excited Rydberg electron, orbiting micrometers away from the nucleus, could be destroyed immediately in a scattering event from a ground state atom. However, energy conservation would require a transition to a neighboring Rydberg state. As the closest states are at least a few GHz apart, orders of magnitude more than the maximum classical energy transfer in such a scattering event, these processes are very unlikely to happen²⁷. The quantization of the Rydberg states here leads to a stabilization of the Rydberg electron at high density. We also verified experimentally that there is no stepwise decay of the Rydberg electron back to the ground state. To this end we measured the BEC atom loss with a $2 \mu\text{s}$ long electric field pulse of variable strength directly after Rydberg excitation and after a $3 \mu\text{s}$ wait. At the end of each sequence we apply another electric field pulse which removes any possibly remaining Rydberg atoms. The sequence is illustrated in the inset of Supplementary Fig. S1. We found that the BEC atom loss starts to vanish at a distinct electric field strength, which is on the order of the classical field ionizing threshold and does not depend on the delay time. From this we can infer that during this $3 \mu\text{s}$, which is a considerable fraction of the measured lifetime of $(5.0 \pm 0.5) \mu\text{s}$, the Rydberg atom is not decaying to states with significantly lower principal quantum numbers. This means that the Rydberg atoms are either decaying directly to relatively low states (as they do for spontaneous decay) or into the continuum. Possible processes could be associative ionization (so called Hornbeck-Molnar ionization) or ion pair formation. In the first process, the Rydberg atom and a neutral ground state atom form a positively charged Rb_2^+ molecular ion; in the latter, a pair of positive and negative Rubidium ions are produced²⁸.

6 Higher order terms in scattering potential

For simplicity the discussion in the main paper is restricted to a constant scattering length a for the interaction of the slow Rydberg electron with the ground state atom. However, as indicated in Fig. 3a there is some correction depending on the momentum $k(R)$ of the electron at distance R from the Rydberg core. The contribution to the s-wave scattering length a is proportional to the polarizability α of the ground state atoms:

$$a(k(\mathbf{R})) = a + \frac{\hbar^2}{e^2 a_0^2 m_e} \cdot \frac{\pi}{3} \alpha k(\mathbf{R}) + O(k^2) \quad (8)$$

To the same order of approximation, the p-wave scattering potential is²⁹:

$$V_p(\mathbf{R}) = -\frac{e^2}{4\pi\epsilon_0} \cdot \frac{2\pi^2}{5} \frac{\alpha}{k(\mathbf{R})} |\nabla\Psi(\mathbf{R})|^2 \quad (9)$$

We obtained the theoretical prediction shown in Fig. 3a by numerically integrating over the s- and p-wave potentials using a semiclassical approximation for the electron momentum¹⁷:

$$k(R) = \sqrt{\frac{2m_e}{\hbar^2} \left(-\frac{Ryd}{(n - \delta_0)^2} + \frac{1}{(4\pi\epsilon_0) R} e^2 \right)} \quad (10)$$

with the Rydberg constant Ryd , the quantum defect δ_0 , and the vacuum permittivity ϵ_0 . As the principal quantum number n of the Rydberg state increases the momentum independent approximation gets better since the mean momentum of the electron is decreasing with $1/n$. Nevertheless, the correction is slightly larger than the error bars of our measurements. However, discrepancies on this order could be equally explained by systematic errors of the measured peak density or the inhomogeneous line broadening due to Rydberg excitation not exactly at the center of the BEC.

7 Coupling to BEC excitations

In the s-wave approximation, the interaction between the electronic density $\rho(\mathbf{r}) = |\Psi(\mathbf{r})|^2$ in the Rydberg nS state and the ground state atoms is described by the interaction potential $V(\mathbf{r}) = g\rho(\mathbf{r})$, where $g = 2\pi\hbar^2 a/m_e$. As the extent of the wavefunction is smaller than the condensate, we can treat the BEC in the thermodynamic limit, assuming a constant atomic density $n(\mathbf{r}) = V^{-1} \sum_{\mathbf{p}, \mathbf{q}} e^{i\mathbf{q}\mathbf{r}} \hat{a}_{\mathbf{p}+\mathbf{q}}^\dagger \hat{a}_{\mathbf{p}}$, where $\hat{a}_{\mathbf{p}}$ is an annihilation operator of a mode \mathbf{p} within the quantization volume V . The interaction can therefore be expressed as a convolution in momentum space

$$\hat{H}_{\text{int}} = g \int d^3r n(\mathbf{r})\rho(\mathbf{r}) = \frac{g}{V} \sum_{\mathbf{p}, \mathbf{q}} \hat{a}_{\mathbf{p}+\mathbf{q}}^\dagger \hat{a}_{\mathbf{p}} \rho_{\mathbf{q}} \quad (11)$$

Using the mean field approximation $\hat{a}_0 \approx \hat{a}_0^\dagger \approx \sqrt{N_0}$, with N_0 denoting the number of atoms in the condensate mode, we can write the interaction in terms of Bogoliubov operators $\hat{b}_{\mathbf{q}} = u_{\mathbf{q}} \hat{a}_{-\mathbf{q}} - v_{\mathbf{q}} \hat{a}_{\mathbf{q}}^\dagger$ as

$$\hat{H}_{\text{int}} \approx \frac{g\sqrt{N}}{V} \sum_{\mathbf{q} \neq 0} \rho_{\mathbf{q}} (u_{\mathbf{q}} - v_{\mathbf{q}}) (\hat{b}_{\mathbf{q}}^\dagger + \hat{b}_{-\mathbf{q}}) \quad (12)$$

where we have neglected constant energy shifts and higher order corrections. Note that within this order of approximation we can replace N_0 by the total atom number N . To estimate the number of excitations induced by the presence of the Rydberg electron with lifetime $\tau = 1/\gamma$ we first consider the probability to excite a certain mode with quasi momentum \mathbf{q} when a perturbation of the type $\hat{H}_{\text{int}} e^{-\gamma t}$ is applied. To lowest order we have

$$P_{0 \rightarrow \mathbf{q}} = \left| -\frac{i}{\hbar} \int_0^\infty dt e^{i\omega_{\mathbf{q}} t - \gamma t} \langle \mathbf{q} | \hat{H}_{\text{int}} | 0 \rangle \right|^2 \quad (13)$$

where the initial state $|0\rangle$ denotes the BEC ground state within Bogoliubov approximation and the final state is given by $|\mathbf{q}\rangle = \hat{b}_{\mathbf{q}}^\dagger |0\rangle$, which is an excited state with energy $E_q = \hbar\omega_q = \sqrt{\epsilon_q^2 + 2\bar{n}g_c\epsilon_q}$. Here we have used the recoil energy $\epsilon_q = \hbar^2q^2/2m_{\text{Rb}}$, the mean density $\bar{n} = N/V$ and the atom-atom coupling constant $g_c = 4\pi\hbar^2a_{\text{Rb}}/m_{\text{Rb}}$ with the s-wave scattering length a_{Rb} . For the probability we now find

$$P_{0\rightarrow\mathbf{q}} = \frac{g^2\rho_{\mathbf{q}}^2}{V^2\hbar^2} \int d\omega S(\mathbf{q}, \omega) |C(\omega)|^2 = \frac{g^2\rho_{\mathbf{q}}^2}{V^2\hbar^2} N \frac{\epsilon_q}{E_q} |C(\omega_q)|^2 \quad (14)$$

where $S(\mathbf{q}, \omega) = N \epsilon_q/E_q \cdot \delta(\omega - \omega_q)$ is the dynamic structure factor of the BEC and $C(\omega) = 1/(\gamma - i\omega)$ is the Fourier transform of the exponential decay. During the time of flight process, the atom-atom interactions quickly become negligible and the Bogoliubov modes are converted into free particles. Using $N = \sum_{\mathbf{p}} \hat{a}_{\mathbf{p}}^\dagger \hat{a}_{\mathbf{p}}$, we find that $\langle \mathbf{q}|N|\mathbf{q}\rangle - \langle 0|N|0\rangle = u_q^2 + v_q^2$ additional particles are in the excited state. The total number of lost atoms ΔN can now be expressed as

$$\Delta N = \sum_{\mathbf{q}} P_{0\rightarrow\mathbf{q}} (u_q^2 + v_q^2) \quad (15)$$

Replacing the sum by an integral and using the healing length $\xi = 1/\sqrt{8\pi\bar{n}a_{\text{Rb}}}$, we have

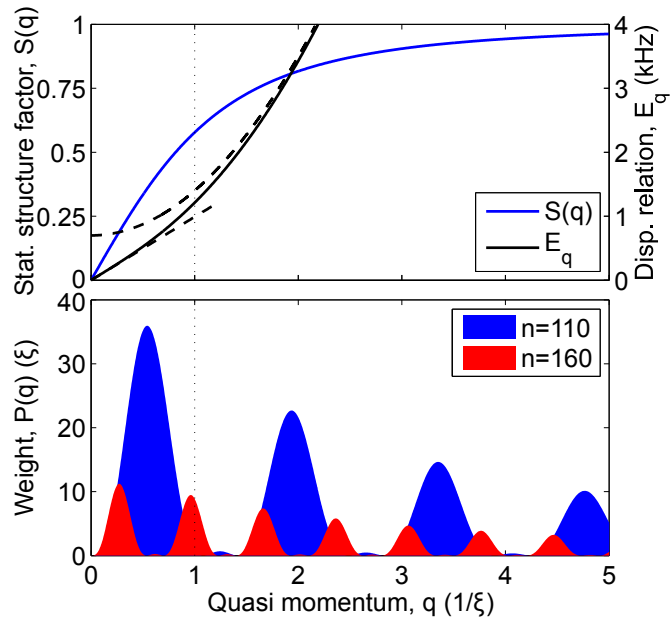
$$\Delta N/\tau^2 = \frac{1}{2\pi^2} \frac{\bar{n}g^2}{\hbar^2} \int dq q^2 \rho_q^2 \frac{1 + (q\xi)^2}{2 + (q\xi)^2} \frac{1}{1 + \omega_q^2/\gamma^2} \quad (16)$$

where we have separated the main dependency on the two measured quantities on the left hand side. Fig. S2 illustrates the nature of the excitations that are generated by the Rydberg electron. The static structure factor $S(\mathbf{q}) = \epsilon_q/E_q$ suppresses excitations at low momenta q . Nonetheless, the excitation weight $P(q) \sim P_{0\rightarrow q}q^2$ shows a clear maximum located at $q \approx 2/R_e < 1/\xi$, where $R_e = 2a_0n^2$ is the radial extent of the Rydberg electron wavefunction. This lies well in the phonon regime for all principal quantum numbers investigated in the experiment. Due to the q^2 factor from the spherical integration there is also a sizable contribution of free particle excitations, which appear as equally spaced peaks with decreasing magnitude.

Some experimental details require extensions to equation (16). First, to account for density inhomogeneities due to the external potential in a simple way we integrate the Thomas-Fermi density profile over the volume which is enclosed by the Rydberg electron, a sphere of radius R_e placed in the center of the atomic cloud. The effective density is then given by the mean value $\bar{n} = (1 - (2R_e/5R_\rho)^2 - (R_e/5R_z)^2) n_0$ on this sphere, where n_0 is the peak density and R_ρ (R_z) is the Thomas-Fermi radius of the cigar shaped BEC in radial (axial) direction. Second, in the experimental sequence, the interaction between the Rydberg electron and the ground state atoms is suddenly terminated after a certain time t_c at which the field ionization occurs. To account for this, the function $C(\omega)$ is modified accordingly:

$$|C(\omega)|^2 = \left| \int_0^{t_c} dt e^{i\omega t - \gamma t} \right|^2 = \frac{1 + e^{-2\gamma t_c} - 2e^{-\gamma t_c} \cos(\omega t_c)}{\gamma^2 + \omega^2} \quad (17)$$

The final correction concerns the way the losses are detected in the experiment. In the absorption images, excitations at small momenta are not distinguished from the condensate fraction due to finite momentum components in the Thomas-Fermi profile. A lower cutoff may thus be introduced in the radial q integration. It turns out that this correction is small and almost all excitations will be detected as losses.



Supplementary Figure 2: Nature of excitations in the condensate. In the upper panel, the static structure factor $S(q)$ of the BEC (blue) is shown together with the Bogoliubov dispersion relation E_q (black), which is shown as a reference. The linear and quadratic regimes are indicated as dashed lines. The lower panel shows the total weight $P(q)$ of excitations at different momenta q for two principal quantum numbers $n = 110$ and 160 .